energies

MDPI

Article

Experimental and Numerical Characterization of the Sliding Rotary Vane Expander Intake Pressure in Order to Develop a Novel Control-Diagnostic Procedure

Fabio Fatigati *, Marco Di Bartolomeo, Davide Di Battista and Roberto Cipollone

Department of Industrial and Information Engineering and Economics, University of L'Aquila, 67100 L'Aquila, Italy; marco.dibartolomeo2@graduate.univaq.it (M.D.B.); davide.dibattista@univaq.it (D.D.B.); roberto.cipollone@univaq.it (R.C.)

* Correspondence: fabio.fatigati@univaq.it; Tel.: +39-0862-434623

Received: 6 May 2019; Accepted: 20 May 2019; Published: 23 May 2019

Abstract: Waste heat recovery via Organic Rankine Cycle (ORC)-based power units represents one of the most promising solutions to counteract the effects of CO_2 emissions on climate change. Nevertheless, several aspects are still limiting its development on the on-the-road transportation sector. Among these aspects, the significant variations of the conditions of the hot source (exhaust gases) are a crucial point. Therefore, the components of the ORC-based unit operate far from the design point if the main operating parameters of the plant are not suitably controlled. The maximum pressure of the cycle is one of the most important variables to be controlled for the importance it has on the effectiveness of the recovery and on safety of operation. In this paper, a wide experimental and theoretical activity was performed in order to define the operating parameters that mostly affect the maximum pressure of the recovery unit. The results showed that the mass flow rate provided by the pump and the expander volumetric efficiency were the main drivers that affect the plant maximum pressure. Subsequently, through a validated model of the expander, a diagnostic map was outlined to evaluate if the expander and, consequently, the whole plant were properly working.

Keywords: ORC-based power unit; waste heat recovery; volumetric expander; expander permeability; ORC diagnostic system

1. Introduction

To date, the transport sector is responsible of 14% of the total amount of anthropogenic greenhouse gas emissions [1], so the efforts of the scientific and technical community are focused on the development of technologies whose introduction allows to reduce this contribution, matching with the increasingly restrictive requests of the international governments and organizations [2,3].

Among the technologies that ensure the CO_2 reduction, waste heat recovery (WHR) from exhaust gases, based on Organic Rankine Cycle (ORC) units, is one of the most attractive alternatives [4]. Indeed, approximately 30% of fuel energy is lost through the exhaust gases [5], whose enthalpy content is almost equal to the engine mechanical useful power [6]. Despite that the ORC-based power unit is a quite conventional technology for stationary applications, it requires some more efforts in the transportation sector, in order to define the most suitable layout, the choice of components, and the level of integration with the engine: Reliability, robustness, and effectiveness in transient situations [7] are the main requirements, taking into account the boundary condition imposed by the specific on board application. Moreover, this application should face issues related to the components encumbrances and weight on a vehicle, backpressure effect on the engine [8,9], proper fitting of the condenser in

the front-end [10], and the devices to be introduced for the final utilization of the recovered power. Considering all these constraints, it is agreed in the literature that a net recovery is around 2–3% of the thermal energy recovered [4], being possible higher recoveries (3–4%) [11] only for heavy duty engines (reduced unsteady behavior).

In fact, the variation of the internal combustion engine (ICE) operating conditions during time and that one of the external parameters (vehicle speed, ambient temperature, driving situations, etc.) produce a severe off design condition of all the components of the recovery unit. The main source of unsteadiness is the high fluctuations of the heat source (exhaust gases in the HRVG) [12]. It is the component that links the high thermal source variations with the remaining ORC components, but it shows a slow time response with respect to expanders and pumps [13]. It is demonstrated that, if the geometry of the heat exchanger is sized to achieve a proper thermal inertia, also without the adoption of control strategies, the fluid is protected by fluctuation of amplitude up to 20 kW and with a frequency not slower than 0.003 Hz [14]. In any case, high evaporator inertia involves disadvantages in the highly dynamic driving cycle with a high engine operating point that does not last long [15].

Concerning the expander machine, several technologies have been proposed. Among turbo-machineries, for instance, radial turbines appears more suitable than axial ones, which suffers so much off-design conditions and needs additional strategies to manage transient state [16,17]. In this regard, volumetric machines seem to better fulfil variable operating requirements [18,19]. Among them, rotary and reciprocating types have been extensively considered. Screw and scroll machines have good robustness to fluctuating conditions [20], while reciprocating ones, which are characterized by a higher built-in volume ratio [21], can achieve more easily a higher expansion ratio and demonstrated very good off-design behavior [22]. Vane machines suffers toughly the leakages [23] due to vane chatter [24], which implies leakages across the adjacent chamber due to the lack of contact between the blade tip and stator [25]. In an ORC based power unit with a volumetric machine as an expander, the machines behavior defines the operating pressure [13], but it can be affected by flow leakages. In fact, if its volumetric efficiency decreases due to leakages, the pump provides a higher mass flow rate being the permeability of the machine increased. If the mass flow rate provided by the pump remains constant, the expander intake pressure (i.e., evaporator outlet pressure) diminishes.

Another operating issue is represented by the cold sink choice that influences the condensing pressure and, consequently, the pressure ratio and power produced by the expander [26]. In particular, the condenser on a vehicle can be cooled by external air, ICE coolant or by a dedicated liquid [27]. In the first case, the condenser acts as a further radiator so its dimensions and frontal area can be relevant. Moreover, the package of the condenser as part of a front-end cooling module represents an engineering challenge as the thermal limits have been quite reached by the current power train cooling components located in a tight under hood environment [28]. On the contrary, in the second and third case, the liquid coolant ensures a downsizing of the condenser but the coolant must be refrigerated by the external air in an additional radiator [29].

In small scale ORC applications, pumps power consumption can severely affect the thermal efficiency and the net power output of the ORC system [30]. However, as pump efficiency is often very low [31], its improved off-design performance can play a key role in the reduction of the back work ratio [32]. Moreover, the cavitation problem can occur in off-design conditions and an overcharging of the working fluid is usually done, leading also to an improvement of the isentropic efficiency of the machine [33]. Variable geometry pumps, finally, can have the possibility to adjust flow rate to the pressure rise needed for ORC control purposes [34,35].

The most common control strategy is to define a constant evaporating temperature (and superheating degree), although in this case it is not possible to define, a priori, which is the one that optimizes the whole process [13]. Good results can be achieved with a control procedure based on the optimization of the evaporating temperature as the function of the condensation one and the thermal conditions of the heat source [13]. Further strategies involve the control of the speeds of the pump and the expander [36] and cooling water mass flow rate [37]. In order to achieve the

evaporating pressure and superheating degree, a first controller constituted by the combination of a dynamic feed-forward and a gain-scheduled proportional integrative derivative (PID) is implemented on the pump [38]. A control system based on a multi-linear approach has also been proposed [39], subdividing the non-linear behavior of the system in local operating regimes as an equivalent linear system. More complex ORC control strategies can also be synthesized, based on a proportional integrative PI controller and involving the coupling of a linear quadratic regulator [40], to keep the many operating parameters within an acceptable limit in the presence of disturbances.

Therefore, an optimal control strategy of an ORC system should consider a detailed off-design model of the components [41,42]. Nonetheless, simpler models seem to be suitable for real time simulation [43] like, for instance, 1D models [44]. Hence, a procedural approach can be used considering only the slowest dynamic (the temperature one) and removes the fastest ones (pump and expander ones), as the time scales associated to the different dynamics vary noticeably [45,46]. Finally, the non-linear behavior of the system can be split into different local operating regimes (multi linear approach) and simpler correlation for the heat transfer can be used. The adoption of a multilinear model allows also to reduce the calibration efforts, using a simple and efficient weighting scheme [47].

In this paper a wide experimental campaign was carried out on a fully instrumented ORC-based power plant bottomed to a 3 liters supercharged diesel engine. It allowed to define the operating parameters that mainly influence the expander intake pressure and its relation with the superheating degree and consequently to the evaporating pressure. Then, an analytic correlation was outlined, which describes the variation of intake pressure and superheating degree as a function of the mass flow rate and expander volumetric efficiency. The experimental data were also compared to the predicted ones provided by a mathematical model of the expander, developed in previous work [48,49]. After its validation, the model was used as a virtual platform to define an expander operating map used for a diagnostic purpose. The map assesses if the expander is not working in accordance to the design expectation due to machine components (blade) wear and damage or incorrect lubrication. Therefore, the developed diagnostic procedure allows us to recognize irregularities on the expander work and to define control strategies to re-establish proper working condition. In this way, also the performance of the whole recovery unit can be preserved as they are very sensitive to the expander operating condition.

2. Materials and Methods

In order to find the main driver that defines the maximum pressure of the ORC-based power, an extensive experimental campaign was performed on a fully instrumented ORC-based power unit bottomed to the exhaust gases of a 3 liters supercharged diesel engine for light duty application. The experimental lay-out, plant components, and the working fluid selected, R236fa, were the same to previous experimental activities [50,51], in order to compare the results.

The ORC-based power unit is constituted by the following components:

(a) A gear pump driven by an electric motor at variable speed;
(b) A plate and fin evaporator designed to reduce the back-pressure effects on the ICE exhaust;
(c) A sliding rotary vane expander;
(d) A plate heat exchanger as condenser.

The working fluid passages are quite conventional in the recovery unit. The variable speed pump delivers a flow rate (proportional to its revolution speed) and the connection with the other components produces a pressure increase. The working fluid enters in the evaporator (plate and fin type) where the heat exchange with the exhaust gases takes place, producing its vaporization. Then, it flows inside the sliding vane rotary expander (SVRE), which is constrained to rotate at 1500 RPM, being connected to an asynchronous generator linked to the electric grid. In Figure 1, the expander adopted is showed and its main properties are reported in Table 1.

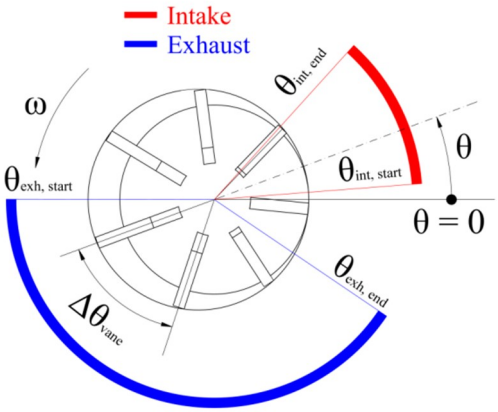

Figure 1. Main dimensions of the sliding rotary vane expander.

Table 1. Sliding rotary vane expander geometry.

Number of Chambers	7
Stator Inner Diameter	75.9 mm
Rotor Outer Diameter	65.0 mm
Eccentricity	5.45 mm
Chamber Width	60.0 mm
Blade Length	17 mm
Blade Thickness	3.96 mm
Angular Vane Extent $\Delta\theta_{vane}$	51.4°
Intake Port Opening Angle $\theta_{int,start}$	4.4°
Intake Port Closing Angle $\theta_{int,end}$	48°
Exhaust Port Opening Angle $\theta_{exh,start}$	180°
Exhaust Port Closing Angle $\theta_{exh,end}$	320°

At the expander exit, it condenses inside a plate heat exchanger cooled by water. A receiver collects the fluid at the suction of the pump, and this dumps flow rates fluctuations and avoid cavitation of the pump, sustaining its intake pressure.

The test bench is fully instrumented in order to measure the thermodynamic quantities entering and leaving each component. The indicated diagram inside the expander was measured thanks to a set of piezo-resistive pressure transducers angularly spaced in order to reconstruct the pressure inside the vanes [51]. The indicated cycle reconstruction allowed a characterization of the expander performance defining its mechanical and volumetric efficiency being additionally measured the shaft torque.

The results of the experimental campaign allowed us to validate a numerical model of the expander developed by the authors [49,51]. Once validated, the model could be used as a virtual platform to predict the expander behavior outside the experimental operating condition. The model was developed in a GT-Suite™ environment and followed an integrated approach between a mono (1-D) and zero-dimensional (0-D) thermo-fluid-dynamic analysis of the working fluid inside the expander. In particular, the (1-D) analysis was adopted to model the filling and emptying phase, which are typically unsteady phenomena. Thus, the intake and exhaust pipes were discretized in multiple sub-volumes in which the mass, momentum, and energy conservations are solved. On the other hand, the 0-D analysis was used to study the fluid behavior inside the vanes, which are so treated as lumped capacities angularly referenced in the direction of rotation. A lumped approach was adopted also to predict the flow leakages through the machine constructive gap. More in details, the leakages between the rotor face and the casing were modeled through an equivalent nozzles while the ones between blade tip and stator and between blade side and slot were described by the Poiseuille-Couette relation, [52] for flow between parallel plates, Equation (1):

$$\dot{m}_{leak,tip} = \rho_{int,end} A \left(\frac{\delta^2 \Delta p}{12 \mu L} + \frac{1}{2} u_{wall} \right) \quad (1)$$

where A is the clearance area, δ is the minimum clearance gap, Δp is the pressure difference between intake and exhaust, μ is the dynamic viscosity, u_{wall} is the relative velocity between the blade tip and stator surface (or between the blade side and rotor slot), L is the length of the leakage path, and $\rho_{int,end}$ is the fluid density at the expander intake end. As δ is hardly evaluable, it was set during the model validation in order to minimize the error between the predicted and experimental mass flow rate, volumetric efficiency, and indicated power [51]. In particular, volumetric efficiency η_{vol} was evaluated according to Equation (2) as the ratio between the mass flow rate introduced inside the vane (expressed as a function of the number of vanes N_v, the revolution speed ω, vane volume $V_{int,end}$ and the density of working fluid $\rho_{int,end}$ at the intake phase) and that provided by the pump:

$$\eta_{vol} = \frac{\dot{m}_{WF,int,end}}{\dot{m}_{WF}} = \frac{N_V V_{int,end} \rho_{int,end} \omega}{\dot{m}_{WF}} \quad (2)$$

The difference between the two streams is due to the volumetric losses, which also affects the indicated power [25] (evaluated through Equation (3)):

$$P_{ind} = \sum_{i=1}^{N_v} \frac{\oint p_i dV_i}{t_{cycle}} \quad (3)$$

where p_i is the pressure inside the vane during rotation, dV_i is the infinitesimal vane volume variation, and t_{cycle} is the time of an expander cycle. Subtracting to P_{ind} the friction losses $P_{mech,lost}$ (quite exclusively due to dry contact between the blade tip and stator) the model allows us to evaluate the mechanical power through Equation (4), which can be compared to the value measured on the shaft.

$$P_{mech} = P_{ind} - P_{mech,lost} \quad (4)$$

Once the mechanical power was evaluated, the global efficiency η_{glob} of the machine can be assessed as the ratio between P_{mech} and the power produced by the machine in adiabatic isentropic condition Equation (5):

$$\eta_{glob} = \frac{P_{mech}}{\dot{m}_{WF}(h_{in} - h_{out,is})} \quad (5)$$

where h_{in} the specific enthalpy of the working fluid at expander intake while $h_{out,is}$ is the specific enthalpy at exhaust in the case of an adiabatic isentropic transformation.

Table 2 reports the validation results of the numerical model: Errors between the predicted and experimental expander intake pressure $p_{exp,in}$ referring to the experimental data were under 8%. The $p_{exp,in}$ was evaluated by the model imposing at the expander inlet the working fluid experimental mass flow rate and its superheating degree, and considering as downstream boundary condition the measured pressure at the expander outlet. Two different sets of tests were performed, with two different values of volumetric efficiencies, obtained by considering different technological clearances of the machines and changing lubrication conditions. The mathematical model was able to accurately reproduce the expander permeability even when its volumetric efficiency decreased. The variation of volumetric efficiency was considered in the model varying δ (Equation (1)) and keeping constant the other constructive gaps. In fact, for the case considered, it was found that the leakages between the blade tip and stator had the greatest influence on volumetric efficiency and on the indicated cycle with respect to the other volumetric losses [51]. Therefore, δ was univocally defined for a certain η_{vol} by the comparison with the experimental results as shown in Table 3.

Table 2. Experimental validation of the numerical mode with η_{vol} = 0.5 and η_{vol} = 0.35.

η_{vol} = 0.5	$p_{exp,in}$ ± 0.3 (bar)	7.0	8.1	8.2	9.2	9.6	10.2	11.1	11.2	11.6	11.4
	Errors on p_{in} (%)	−2.5	−4.9	3.8	−0.2	0.1	3.0	3.5	4.0	2.4	5.7
η_{vol} = 0.35	$p_{exp,n}$ ± 0.3 (bar)	5.4	6.8	7.3	7.7	8.6	9.4	7.7	8.8	10.4	10.9
	Errors on p_{in} (%)	−5.5	−6.0	0.6	−3.4	−1.0	0.6	−3.5	2.9	5.2	8.2

Table 3. Minimum clearance gaps set.

Minimum Clearance Gap Set	η_{vol} = 0.5	η_{vol} = 0.35
Clearance gap between blade tip and stator	85 μm	140 μm
Clearance gap between vane side and slot	5 μm	5 μm
Diameter of equivalent orifice (leakages across covers)	0.2 mm	0.2 mm

3. Results and Discussion

The experimental analysis consented to determine the influence of the operating parameters on the evaporating pressure and consequently that one at the expander intake. These pressure values were fixed by the combined operation of the expander revolution speed and the mass flow rate provided by the pump. In particular, the evaporating pressure raises increasing the mass flow rate or decreasing the expander revolution speed, leading often also the reduction of the superheating degree [53]. Therefore, if the expander revolution speed does not change, it is fundamental to evaluate how the working fluid flow rate influences the evaporating pressure, having guaranteed a given superheating degree.

In Figure 2a the values of the expander intake pressure are reported as a function of the mass flow rate for different ranges of the working fluid superheating degree. As Figure 2a shows, the pressure was not influenced by this parameter, demonstrating a substantial linear behavior with mass flow rate. Indeed, if the mass flow rate varied between 0.070 kg/s and 0.125 kg/s, the intake pressure rose linearly within the range 7–12 bar, in despite of the working fluid superheating degree (between 0 °C and 20 °C). Therefore, the mass flow rate was the main driver that defines almost univocally the expander intake pressure. In order to ensure the specified superheating degree, the thermal power exchanged between exhaust gases and working fluid changes as it is reported in Figure 2b. In Table 4, some experimental cases of Figure 2 are reported in more detail. It can be noticed how the increase of intake pressure led to an enhancement of the mechanical power produced by the expander as the indicated power grows.

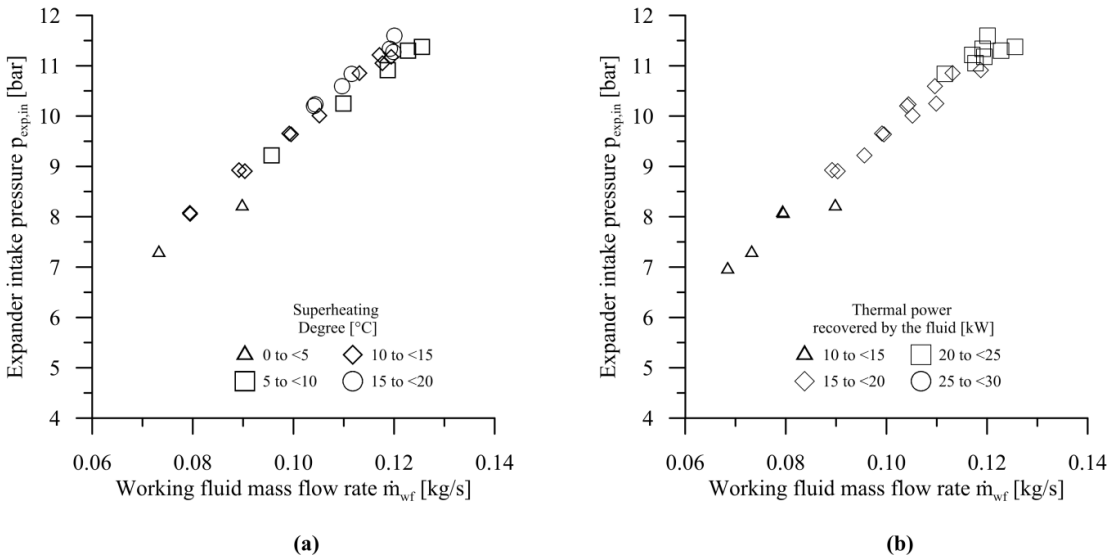

Figure 2. (**a**) Intake pressure varying the mass flow rate for different values of superheating degree; and (**b**) intake pressure varying the mass flow rate for different values of thermal power recovered.

Table 4. Experimental characterization of the expander when η_{vol} = 0.5.

Case	1	2	3	4	5	6	7	8	9	10
$\omega \pm 1$ (RPM)	1515	1518	1517	1525	1526	1529	1531	1534	1537	1535
P_{mech} (W)	281	361	340	471	471	559	566	625	693	629
$T_{in} \pm 0.3$ (°C)	83	74	63	74	80	79	87	88	96	83
$T_{out} \pm 0.3$ (°C)	63	51	42	54	62	62	71	72	79	68
$p_{exp,in} \pm 0.3$ (bar)	7.0	8.1	8.2	9.2	9.6	10.2	11.1	11.2	11.6	11.4
$p_{exp,out} \pm 0.3$ (bar)	3.4	3.7	3.9	4.1	4.4	4.5	4.9	4.8	4.8	4.9
$\dot{m}_{WF} \pm 0.15\%$ (kg/s)	0.069	0.079	0.089	0.096	0.099	0.110	0.118	0.120	0.120	0.125
η_{vol}	0.48	0.49	0.48	0.47	0.47	0.46	0.46	0.45	0.45	0.46
η_{glob}	0.33	0.37	0.34	0.39	0.37	0.39	0.36	0.38	0.39	0.38

The mechanical power produced by the expander increased from 281 W to 629 W when the intake pressure rose from 7 bar to 11.4 bar. Nevertheless, for the same mass flow rate, the expander outlet pressure increased from 3.4 bar to 4.9 bar causing a negative effects on the indicated power and on the mechanical power. Among the two effects, the one associated to the pressure increase was greater than that one related to the expander backpressure increase and, definitively, the mechanical power rises with mass flow rate provided by the pump. Concerning the performance of the machine, the average volumetric (evaluated according Equation (2)) and global efficiency (evaluated according Equation (4)) of the expander was in the 0.37–0.47 range.

Thus, when the expander revolution speed is constant, the dependence of the intake pressure on the mass flow rate is quite linear considering stationary conditions. Nevertheless, also the volumetric efficiency of the expander plays an important role in the definition of the evaporating pressure. Indeed, as reported in [25], if the volumetric efficiency decreases due to the leakages across constructive gap, for a fixed mass flow rate provided by the pump and no control valve downstream the evaporator, the expander intake pressure (and consequently the evaporating one) decreases. Therefore, in this case, part of the mass by-passes the vanes and flows towards the adjacent chamber or directly to the exhaust. In order to deepen the effects of volumetric efficiency decrease on the evaporating pressure, a further experimental campaign was carried out on the same machine with a lower volumetric efficiency (η_v = 0.35).

The results are reported in Table 5 show that a wider range of mass flow rate is needed (0.075–0.171 kg/s) to ensure the intake pressure (ranging between 5.4 bar and 10.9 bar). On the other hand if, the volumetric efficiency decreases down to 0.35, global efficiency also decreases to a mean value of 0.30 (Table 5). Therefore, the linear growth of the intake pressure with mass flow rate had a lower slope as can be seen in Figure 3a. This slope depends on the permeability of the expander, which is defined as the ratio between the mass flow rate and the intake pressure expressed as in Equation (6). Thus, the higher was the expander permeability, the lower was the intake pressure in correspondence of a same mass flow rate provided by the pump.

$$\alpha = \frac{\dot{m}_{WF}}{p_{exp,in}} \tag{6}$$

This means also that, for a fixed intake pressure, the mass flow rate circulating inside the plant was higher as the pressure drop caused by the expander was lower. However, the higher fraction of mass flow rate flows quite entirely towards adjacent chambers or to exhaust without producing work. Moreover, the increase of volumetric losses led to a higher thermal power needed at the evaporator to guarantee the same superheating degree ΔT_{SH} for a given expander intake pressure (Figure 3b). Indeed, the machine with higher volumetric losses had greater permeability, so to guarantee the same intake pressure the mass flow rate provided by the pump must increase and the thermal energy recovered at the evaporator raises. It is worthy to observe that the extra mass flow rate, sent by the pump to overcome the higher volumetric losses of the expander, not completely by-passes the expander. Indeed,

the mass flow rate, which flows from the suction vane to the adjacent one (in the verse of rotation), sustains the initial expansion pressure and consequently produces a positive effect on indicated power. This means that this kind of leakage worsens the filling of the suction chamber, but ensures to feed the adjacent one, which is expanding. Thus, the leaked mass is not completely lost and produces a recovery effects. For this reason, the volumetric losses increase certainly worsens the global efficiency, but the mass recirculation between adjacent vanes produces a positive effect, which partially compensates the efficiency penalty.

Table 5. Experimental characterization of the expander with η_{vol} = 0.35.

Case	1	2	3	4	5	6	7	8	9	10
w ± 1 (RPM)	1509	1521	1524	1528	1534	1539	1529	1534	1544	1545
P_{mech} (W)	202	401	446	511	601	691	540	650	816	838
T_{in} ± 0.3 (°C)	49	67	61	75	76	81	73	75	84	81
T_{out} ± 0.3 (°C)	35	52	46	57	60	64	59	58	66	63
$p_{exp,in}$ ± 0.3 (bar)	5.4	6.8	7.3	7.7	8.6	9.4	7.7	8.8	10.4	10.9
$p_{exp,out}$ ± 0.3 (bar)	2.6	2.8	3.0	3.0	3.3	3.5	2.9	3.2	3.6	3.8
$\dot{m}_{WF}$ ± 0.15% (kg/s)	0.075	0.091	0.107	0.107	0.121	0.135	0.106	0.129	0.157	0.171
η_{vol}	0.36	0.35	0.34	0.36	0.35	0.33	0.34	0.34	0.34	0.33
η_{glob}	0.24	0.31	0.30	0.31	0.32	0.32	0.32	0.31	0.30	0.30

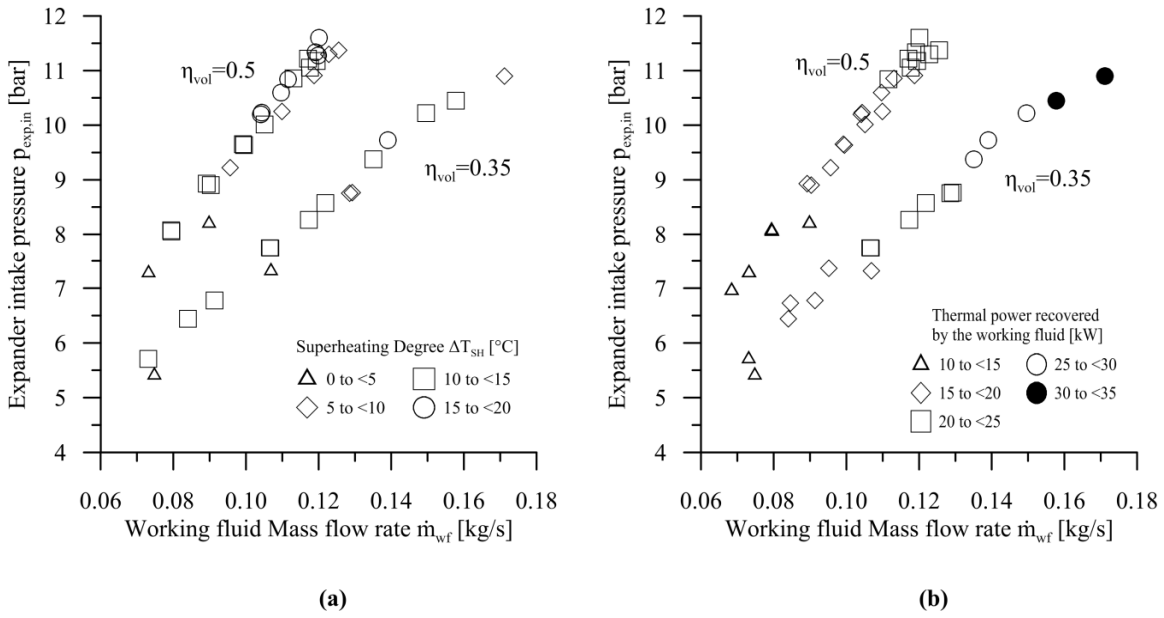

Figure 3. (**a**) Effect of the expander volumetric efficiency on intake pressure variation as a function of the mass flow rate for different values of superheating degree; and (**b**) effect of the expander volumetric efficiency on the thermal power recovered by the working fluid.

The quite linear dependence of the intake pressure on the mass flow rate provided by the pump shows a scarce influence of the superheating degree on $p_{exp,in}$. This behavior can be theoretically explained, starting from the mass conservation applied to the expander (Equation (7)), obtained by rearranging Equation (2):

$$\dot{m}_{WF} = \frac{N_V V_{int,end} \rho_{int,end} \omega}{\eta_{vol}} \tag{7}$$

Subsequently, the density of the working fluid can be explicated and Equation (8) can be written:

$$\rho_{int,end} = \frac{\eta_{vol} \dot{m}_{WF}}{N_V V_{int,end} \omega} \tag{8}$$

The relation shows how increasing $\dot{m}_{WF}$, the working fluid density must increase almost linearly if the expander revolution speed is constant. In fact, the remaining terms are all constant: N_v and $V_{int,end}$ are the geometric parameter and η_v depends on the minimum clearance gap between the vane tip stator and inner stator surface and between the rotor and expander covers. Therefore, the density of the fluid must match Equation (8), rearranging in some way the local inlet temperature of the working fluid.

Considering the ideal gas law, corrected by the compressibility factor to take into account the real behavior of the working fluid, the intake pressure can be expressed as a function of $\rho_{int,end}$ (Equation (9)):

$$\frac{p_{int,end}}{\rho_{int,end}} = ZR\left(T_{vap}\left(p_{exp,in}\right) + \Delta T_{SH}\right) \tag{9}$$

In Equation (9), the fluid temperature is expressed as the sum of the vaporization temperature, depending on the intake pressure $p_{exp,in}$, and the superheating degree ΔT_{SH}, in order to assess the influence of the latter on the intake pressure variation. Equation (9) shows how the influence of superheating on the ratio between the intake pressure and density of the working fluid is negligible, as T_{vap} is considerably greater than ΔT_{SH}. Introducing Equation (8) in Equation (9), the dependence between the intake pressure and the mass flow rate provided by the pump can be expressed according to Equation (10).

$$p_{int,end} = Z\frac{R\left(T_{vap}\left(p_{exp,in}\right) + \Delta T_{SH}\right)\eta_{vol}}{N_V V_{int,end}\omega}\dot{m}_{WF} \tag{10}$$

Equation (10) represents the effect of the mass flow rate variation on the pressure inside the vane at the end of the intake phase. However, in order to consider the pressure at expander inlet (evaporator pressure) $p_{exp,in}$, the pressure drop caused by the intake phase (which does not proceed as an isobaric transformation and it is also affected by the unavoidable intake section restriction) should be taken into account. Thus, $p_{exp,in}$ can be expressed by Equation (11):

$$p_{exp,in} = Z\frac{RT_{in}\eta_{vol}}{N_V V_{int,end}\omega}\dot{m}_{WF} + k_{\Delta p,int}\dot{m}_{WF} \tag{11}$$

where $k_{\Delta p,int}$ is an empiric coefficient coming from the linearization of the experimental behavior of the pressure drop for the considered mass flow rate range. Equation (11) shows as the main parameters that affects $p_{exp,int}$ are the mass flow rate, expander revolution speed, and volumetric efficiency. In general, volumetric efficiency depends on the expander revolution speed, however, in this work ω is constant and η_{vol} depends only on the clearance width and lubrication condition. Equation (11) theoretically explains the experimental result conducted with different η_{vol}. In fact, if η_{vol} decreases the angular coefficient of Equation (11) diminishes demonstrating the reduction of the slope of the linear increase of $p_{exp,in}$ as a function of $\dot{m}_{WF}$. It is worth observing that in Equation (11), in order to obtain a linear relation, the inlet temperature T_{in} was not expressed as a function of the evaporating pressure. In fact, the evaporating pressure p_{evap} can be obtained as in Equation (12) adding to $p_{exp,in}$ (coming from Equation (11)) the pressure drop across the evaporator Δp_{HRVG}.

$$p_{evap} = p_{exp,in} + \Delta p_{HRVG} \tag{12}$$

Obviously, if Δp_{HRVG} is lower, pressure drops across the evaporator are negligible with respect to the evaporating pressure. In fact, among the components of the ORC-based power unit, the expander is the less permeable as can be observed from Figure 4a, where the pressure drops across each component are reported. Therefore, the evaporating pressure is mainly defined by the expander permeability (Figure 4b) only if its permeability is lower than those of the other components. Nevertheless, this always happens if the evaporator and condenser have been properly designed.

Moreover, also the effects of the variation of the expander outlet pressure $p_{exp,out}$ on the expander permeability can be observed, particularly due to the numerical model. The variation of $p_{exp,out}$ is very

frequent in WHR in the automotive sector because the conditions of the cold source, on which depends $p_{exp,out}$, can change significantly. In the experimental campaign $p_{exp,out}$ varies within a narrow range (3–5 bar) and its effect on expander intake pressure cannot be observed.

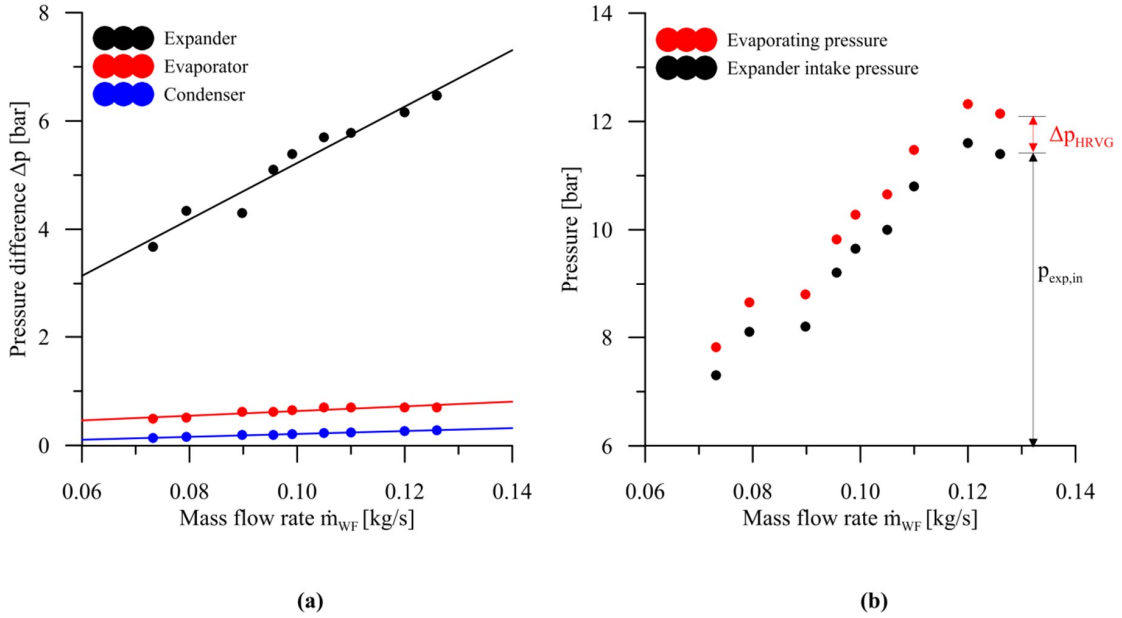

(a) **(b)**

Figure 4. (**a**) Pressure drop across the evaporator, condenser, and expander varying the mass flow rate; and (**b**) evaporating and expander intake pressure varying the mass flow rate provided by the pump.

Thus, due to the validated virtual platform, the expander intake pressure was evaluated as a function of the mass flow rate, varying $p_{exp,out}$. In Figure 5a the intake pressure as a function of the mass flow rate was reported for the expander with η_{vol} = 50% while in Figure 5b the result of the same analysis was showed when η_{vol} = 35%. The values of $p_{exp,out}$ considered were 3 bar, 5 bar, and 7 bar. As can be noticed from Figure 5a even if $p_{exp,out}$ varies, the intake pressure trend as a function of $\dot{m}_{WF}$ is not affected by the $p_{exp,out}$ increase.

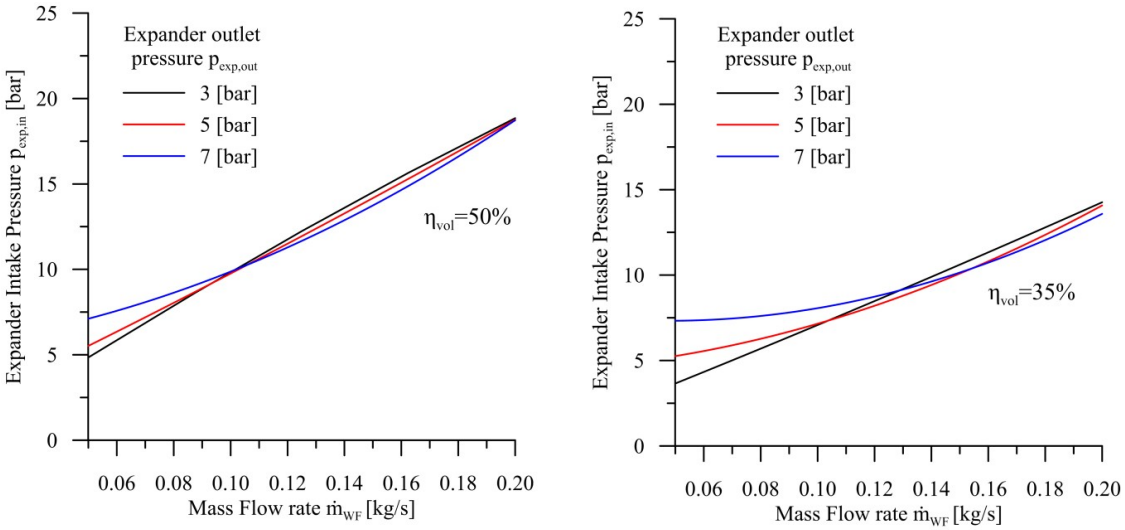

(a) **(b)**

Figure 5. Expander intake pressure varying the mass flow rate provided by the pump and the expander outlet pressure when the expander volumetric efficiency is η_{vol} = 50% (**a**) and η_{vol} = 35% (**b**).

On the contrary, for the machine with lower volumetric efficiency when the $p_{exp,out}$ was equal to 7 bar, the intake pressure trend was far from that corresponding to the cases in which $p_{exp,out}$ ranges between 3 bar and 5 bar. In particular, the increase of $p_{exp,out}$ led to higher intake pressure, keeping constant the $\dot{m}_{WF}$ considered. This happens when the machine has a lower volumetric efficiency because the clearance gaps are higher. Indeed, if the expander had not clearance (η_{vol} = 1) the communication between the intake and exhaust would not take place and $p_{exp,out}$ cannot influence the expander intake pressure. Thus the expander ideally breaks the whole circuit in two parts: A higher pressure side upstream the machine and a lower pressure side downstream it. Nevertheless, a clearance gap cannot be avoided in real construction, to guarantee the expander functionality and a communication between the intake and exhaust port happen. Therefore, the higher the clearance gap is the larger are the effects of $p_{exp,out}$ on intake pressure.

A Model Based Diagnostic Procedure for SVRE

The virtual platform allowed to represent the whole operating range covered by the machine in a control map as reported in Figure 6. In order to define control strategies, the use of the map can be more feasible than a real time model prediction in order to be stored in a conventional engine electronic control unit (ECU) [47].

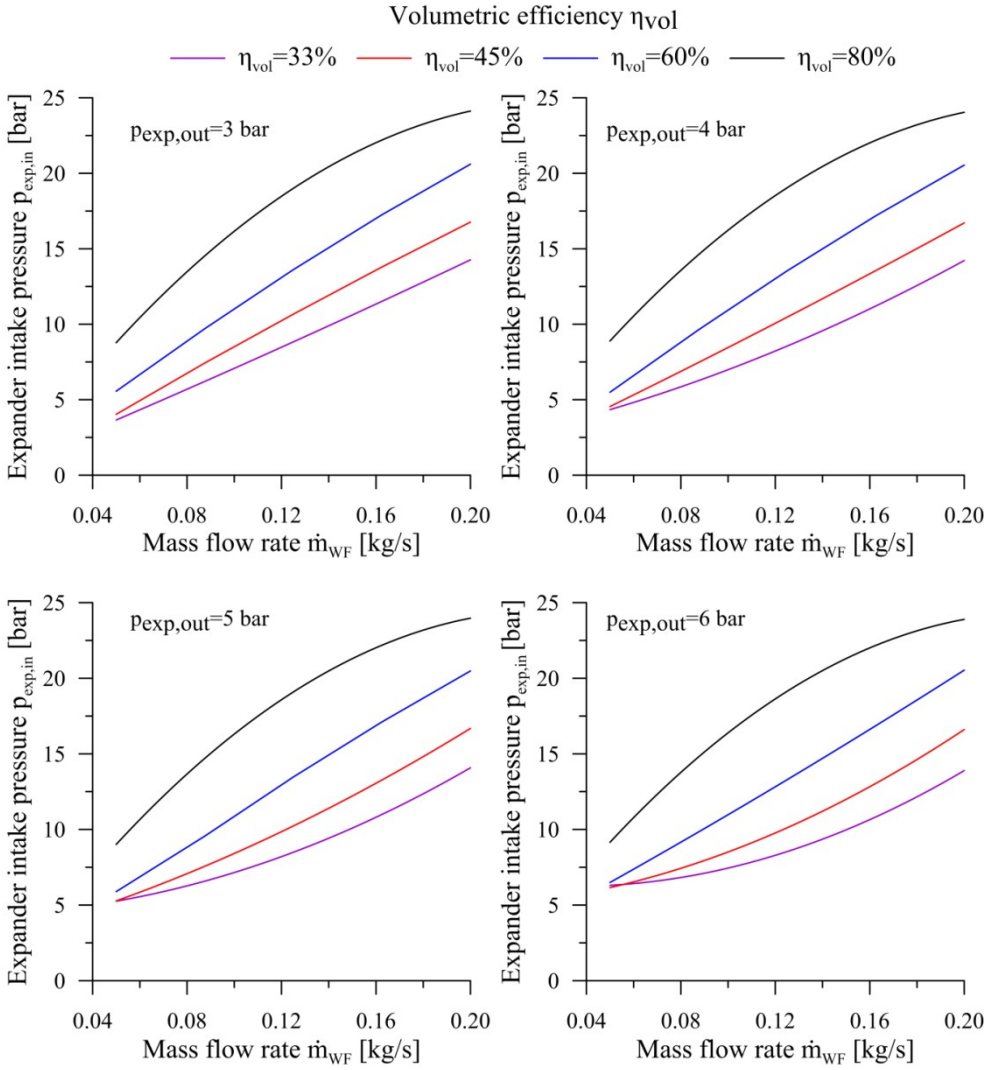

Figure 6. Diagnostic map of the expander operating condition.

The maps reported in Figure 6 allow to evaluate if the expander is working according to the expected condition or if anomalies are taking place. The maps represent the intake pressure trend as a function of $\dot{m}_{WF}$ provided by the pump for different values of volumetric efficiency of the expander. In order to consider also the effects of the condensing pressure on the intake pressure of the expander, a diagnostic map can be derived for several $p_{exp,out}$. Therefore, entering the intake and exhaust pressure of the expander and the mass flow rate circulating inside the plant, the map detects if the expander is properly working. In fact, referring to Figure 6, once the $p_{exp,out}$ is known (by a measurement), the corresponding sub-map can be considered. From it, the evaluation of the expander volumetric efficiency can be univocally performed entering the intake pressure and mass flow rate measured.

If the actual volumetric efficiency is lower than the designed expectations, an incorrect lubrication or clearance gap increase (due to wear or damages of the components) could be happened. Moreover, the map can be used also for control purposes: Once the volumetric efficiency is known, it allows us to predict which is the mass flow rate needed to achieve a certain intake pressure value. Nevertheless, if the thermal energy available at a hot thermal source does not change, the intake pressure of the expander cannot be regulated acting only on the mass flow rate. Keeping constant the expander revolution speed, if the mass flow rate is increased to rise the intake pressure, the superheating degree of the working fluid at the expander inlet decreases down to an extreme condition, in which the working fluid no longer completely vaporizes. On the other hand, if the mass flow rate decreases to reduce the intake pressure, the temperature of the working fluid can exceed its stability limits. Therefore, a further control parameter represented by the regulation of the expander speed is required. The expander revolution speed control can be electrically or mechanically achieved, it requires an additional control strategy increasing the system complexity. However, it allows widening in the flexibility of the ORC-based power unit and to control it, reducing the variation of the mass flow rate. Indeed, keeping constant the mass flow rate entering in the expander, if the expander revolution speed ω decreases, the pressure increases. Meanwhile, if ω increases the intake pressure diminishes. This is also confirmed by the Equation (11), indeed a decrease of ω leads to an increase of the linear trend slope of intake pressure with mass flow rate. Therefore, the combination of the growth of mass flow rate provided by the pump and the decrease of expander revolution speed leads to an increase of intake pressure, causing a reduction of the superheating degree. The best configuration of the mass flow rate and expander revolution speed should be selected in order to optimize the cycle performance [53]. In fact, when the expander revolution speed varies the effect on the expander efficiency should be taken into account: The expander revolution speed reduction has an opposite effect on volumetric and mechanical efficiencies. Indeed, the volumetric efficiency diminishes as the centrifugal force and, consequently, the sealing action on the blade, decreases. On the other hand, the mechanical efficiency increases because the dry friction between the blade and stator is reduced. Therefore, when the expander revolution speed is varied, the potential detrimental effects on expander efficiency should be assessed. Although in this paper the map was outlined for a fixed ω, it is able to consider also the variation of ω and its impact on expander efficiency. This allows us to evaluate the combined effect on the intake pressure of the mass flow rate and expander revolution speed, in order to define a suitable control strategy.

4. Conclusions

In this work, experimental and numerical activities were performed in order to assess the main operating quantities that define the expander intake pressure and consequently the ORC-based power unit evaporating pressure. A wide experimental campaign was conducted on an ORC-based power unit fed by the exhaust gas of a 3 literssupercharged diesel engine. The mass flow rate circulating inside the ORC was varied by changing the pump speed, while the expander rotational speed was fixed as the generator was connected to electric grid. The results were carried out for the expander with different volumetric efficiency (0.5 and 0.35). The following experimental evidences were observed:

(a) The intake pressure of the expander tended to linearly increase with the mass flow rate provided by the pump, even if the superheating degree varied. The ratio between mass flow rate at the intake pressure and the mass flow rate provided by the pump was defined as permeability.
(b) The permeability of the machine increased if the expander volumetric efficiency decreased. In fact, the slope of the linear trend of the expander intake pressure, when the mass flow rate increased, diminished with the lowering of the volumetric efficiency, so keeping constant the mass flow rate circulating inside the plant and, consequently, the energy recovered from the upper thermal source, the expander intake pressure depends only on the expander volumetric efficiency, if its revolution speed remains constant.
(c) The expander permeability fixed the evaporating pressure of the ORC-based power unit if the evaporator and condenser have a pressure drop quite negligible with respect to the expander, as it happens if the heat exchangers are properly conceived.

These experimental evidences were confirmed also by an analytical relation, which demonstrates that the superheating degree of the working fluid has a scarce influence on the expander intake pressure with respect to the mass flow rate and expander revolution speed.

Due to the wide experimental data, a numerical model of the expander was validated and used as a virtual platform to analyze the expander behavior for the operating condition outside the range considered during the experimental campaign. In particular the effects of the expander outlet pressure variation on the intake one was observed demonstrating that, if the clearance gap are high (lower volumetric efficiency), the linear intake pressure trend results slightly modified. Hence, a diagnostic map that covers the entire possible expander operating region was outlined. Measuring the value of discharge and intake pressure of the expander, and knowing the value of mass flow rate delivered by the pump, the map allows us to estimate the volumetric efficiency of the machine, assessing if wear, damages, or incorrect lubrication occurred. This can be useful also to determine the maintenance time of the component. Finally, the map can be used also for control purposes: It allows us to define the mass flow rate required to achieve a certain intake pressure, once the maintenance conditions are predicted. Despite this map was referred in this paper to a fixed expander revolution speed, it can be outlined also varying this parameter. This allows us to observe the combined effects of the expander revolution speed and mass flow rate on the intake pressure. In fact, a control of the intake pressure, based only on the mass flow rate variation, cannot be feasible if its variation is high and the thermal energy of the hot source does not change. Therefore, the intake pressure should be regulated acting also on the variation of the expander revolution speed to mitigate the mass flow rate fluctuation.

Author Contributions: Conceptualization, F.F. and R.C.; methodology, D.D.B., software, F.F.; validation and investigation, M.D.B., F.F. and D.D.B.; resources, R.C.; data curation, F.F. and M.D.B.; writing—original draft preparation, F.F.; writing—review and editing, D.D.B.; visualization, F.F. and D.D.B.; supervision, R.C.

Funding: This research received no external funding, all the acknowledgments have been given in the next section.

Acknowledgments: The author are grateful to Giulio Contaldi, CEO of Ing. Enea Mattei S.p.A. and Stefano Murgia, Director of Research and Development department of Ing. Enea Mattei S.p.A. for the support giving during this research activity.

Conflicts of Interest: The authors declare no conflict of interest. "The funders had no role in the design of the study; in the collection, analyses, or interpretation of data; in the writing of the manuscript, or in the decision to publish the results".

Nomenclature

A	Leakage Area (mm^2)
ECU	Engine Electronic Control Unit
HRVG	Heat Vapor Recovery Generator
ICE	Internal Combustion Engine
k	Empiric coefficient for pressure drop
L	Length (m)
$\dot{m}$	Working fluid mass flow rate (kg/s)

N_v	Vane Number
P	Power (W)
PID	Proportional Integrative Derivative
ORC	Organic Rankine Cycle
R	Individual gas constant (J/kgK)
SVRE	Sliding Vane Rotary Expander
u	Working fluid velocity (m/s)
V	Volume (m^3)
W	Width (mm)
Z	Compressibility factor
WHR	Waste Heat Recovery
Sub-scripts:	
exp,in	Expander inlet
exp,in	Expander outlet
leak,tip	Leak flow at tip blade
mech	Mechanical power
mech,lost	Mechanical power lost
p	Pressure drop coefficient
SH	Super heating
vap	Vaporization
vol	Volumetric efficiency
wall	Stator inner wall
WF	Working Fluid
Greek symbols:	
α	Expander permeability
δ	Clearance between blade and stator (μm)
Δp	Discrete pressure difference (Mpa)
η	Efficiency
μ	Dynamic viscosity (Pa·s)
ρ	Working fluid density (kg/m^3)
ω	Expander revolution speed (rpm), (rad/s)

References

1. Edenhofer, O.; Pichs-Madruga, R.; Sokona, Y.; Farahani, E.; Kadner, S.; Seyboth, K.; Adler, A.; Baum, I.; Brunner, S.; Eickemeier, P.; et al. (Eds.) IPCC, 2014: Summary for Policymakers. In *Climate Change 2014: Mitigation of Climate Change. Contribution of Working Group III to the Fifth Assessment Report of the Intergovernmental Panel on Climate Change*; Cambridge University Press: Cambridge, UK; New York, NY, USA, 2014.
2. Regulation (EC). *No. 443/2009 of the European Parliament and of the Council of 23 April 2009, Setting Emission Performance Standards for New Passenger Cars as Part of the Community's Integrated Approach to Reduce CO2 Emissions from Light-Duty Vehicles*; European Parliament, Council of the European Union, Official Journal of the European Union: Brussels, Belgium, 2009.
3. Regulations Regulation (Eu). *No 510/2011 of the European Parliament and of the Council of 11 May 2011 Setting Emission Performance Standards for New Light Commercial Vehicles as Part of the Union's Integrated Approach to Reduce CO2 Emissions from Light-Duty Vehicles*; European Parliament, Council of the European Union, Official Journal of the European Union: Brussels, Belgium, 2011.
4. Cipollone, R.; di Battista, D.; Bettoja, F. Performances of an ORC power unit for Waste Heat Recovery on Heavy Duty Engine. *Energy Procedia* **2017**, *129*, 770–777. [CrossRef]
5. Koppauer, H.; Kemmetmüller, W.; Kugi, A. Modeling and optimal steady-state operating points of an ORC waste heat recovery system for diesel engines. *Appl. Energy* **2017**, *206*, 329–345. [CrossRef]
6. di Battista, D.; Mauriello, M.; Cipollone, R. Waste heat recovery of an ORC-based power unit in a turbocharged diesel engine propelling a light duty vehicle. *Appl. Energy* **2015**, *152*, 109–120. [CrossRef]

7. Guillaume, L.; Legros, A.; Desideri, A.; Lemort, V. Performance of a radial-inflow turbine integrated in an ORC system and designed for a WHR on truck application: An experimental comparison between R245fa and R1233zd. *Appl. Energy* **2017**, *186*, 408–422. [CrossRef]
8. di Battista, D.; di Bartolomeo, M.; Villante, C.; Cipollone, R. On the limiting factors of the waste heat recovery via ORC-based power units for on-the-road transportation sector. *Energy Convers. Manag.* **2018**, *155*, 68–77. [CrossRef]
9. Espinosa, N.; Tilman, L.; Lemort, V.; Quoilin, S.; Lombard, B. Rankine cycle for waste heat recovery on commercial trucks: Approach, constraints and modelling. In *SIA, Diesel International Conference and Exhibition*; France, 2010; Available online: http://hdl.handle.net/2268/62995 (accessed on 1 May 2019).
10. Di Battista, D.; Di Bartolomeo, M.; Villante, C.; Cipollone, R. A Model Approach to the Sizing of an ORC Unit for WHR in Transportation Sector. *SAE Int. J. Commer. Veh.* **2017**, *10*. [CrossRef]
11. Yang, C.; Xie, H.; Zhou, S. Efficiency Analysis of the Rankine Cycle System Used for Engine Exhaust Energy Recovery Under Driving Cycle. *SAE Int. Paper* **2014**. [CrossRef]
12. Sun, H.; Qin, J.; Hung, T.C.; Huang, H.; Yan, P.; Lin, C.H. Effect of flow losses in heat exchangers on the performance of organic Rankine cycle. *Energy* **2019**, *172*, 391–400. [CrossRef]
13. Quoilin, S.; Aumann, R.; Grill, A.; Schuster, A.; Lemort, V.; Spliethoff, H. Dynamic modeling and optimal control strategy of waste heat recovery Organic Rankine Cycles. *Appl. Energy* **2011**, *88*, 2183–2190. [CrossRef]
14. Jiménez-Arreola, M.; Wieland, C.; Romagnoli, A. Direct vs indirect evaporation in Organic Rankine Cycle (ORC) systems: A comparison of the dynamic behavior for waste heat recovery of engine exhaust. *Appl. Energy* **2019**, *242*, 439–452. [CrossRef]
15. Grelet, V.; Reiche, T.; Lemort, V.; Nadri, M.; Dufour, P. Transient performance evaluation of waste heat recovery rankine cycle-based system for heavy duty trucks. *Appl. Energy* **2016**, *165*, 878–892. [CrossRef]
16. Di Battista, D.; Cipollone, R. Experimental analysis of an organic Rankine cycle plant bottoming a heavy-duty engine using axial turbine as prime mover. *SAE Int. J. Engines* **2017**, *10*, 1385–1397. [CrossRef]
17. Sun, H.; Qin, J.; Hung, T.C.; Huang, H.; Yan, P. Performance analysis of low speed axial impulse turbine using two type nozzles for small-scale organic Rankine cycle. *Energy* **2019**, *169*, 1139–1152. [CrossRef]
18. Imran, M.; Usman, M.; Park, B.S.; Lee, D.H. Volumetric expanders for low grade heat and waste heat recovery applications. *Renew. Sustain. Energy Rev.* **2016**, *57*, 1090–1109. [CrossRef]
19. Pantano, F.; Capata, R. Expander selection for an on-board ORC energy recovery system. *Energy* **2017**, *141*, 1084–1096. [CrossRef]
20. Dumont, O.; Parthoens, A.; Dickes, R.; Lemort, V. Experimental investigation and optimal performance assessment of four volumetric expanders (scroll, screw, piston and roots) tested in a small-scale organic Rankine cycle system. *Energy* **2018**, *165*, 1119–1127. [CrossRef]
21. Bianchi, M.; Branchini, L.; Casari, N.; De Pascale, A.; Melino, F.; Ottaviano, S.; Pinelli, M.; Spina, P.R.; Suman, A. Experimental analysis of a micro-ORC driven by piston expander for low-grade heat recovery. *Appl. Therm. Eng.* **2019**, *148*, 1278–1291. [CrossRef]
22. Chatzopoulou, M.A.; Simpson, M.; Sapin, P.; Markides, C.N. Off-design optimisation of organic Rankine cycle (ORC) engines with piston expanders for medium-scale combined heat and power applications. *Appl. Energy* **2019**, *238*, 1211–1236. [CrossRef]
23. Yang, B.; Peng, X.; He, Z.; Guo, B.; Xing, Z. Experimental investigation on the internal working process of a CO2 rotary vane expander. *Appl. Therm. Eng.* **2009**, *29*, 2289–2296. [CrossRef]
24. Badr, O.; Probert, S.D.; O'Callaghan, P. Performances of Multi-Vane Expanders. *Appl. Energy* **1985**, *20*, 207–234. [CrossRef]
25. Vodicka, V.; Novotny, V.; Mascuch, J.; Kolovratnik, M. Impact of major leakages on characteristics of a rotary vane expander for ORC. *Energy Procedia* **2017**, *129*, 387–394. [CrossRef]
26. Garg, P.; Karthik, G.M.; Kumar, P.; Kumar, P. Development of a generic tool to design scroll expanders for ORC applications. *Appl. Therm. Eng.* **2016**, *109*, 878–888. [CrossRef]
27. Cipollone, R.; di Battista, D.; Gualtieri, A. A novel engine cooling system with two circuits operating at different temperatures. *Energy Convers. Manag.* **2013**, *75*, 581–592. [CrossRef]
28. Dickson, J.; Ellis, M.; Rousseau, T.; Smith, J. Validation and design of heavy vehicle cooling system with waste heat recovery condenser. *SAE Int. J. Commer. Veh.* **2014**, *7*, 458–467. [CrossRef]
29. Cipollone, R.; Di Battista, D.; Gualtieri, A.; Massimi, M. Development of Thermal Modeling in Support of Engine Cooling Design. *SAE Technical Paper* **2013**. [CrossRef]

30. Bianchi, G.; Fatigati, F.; Murgia, S.; Cipollone, R.; Contaldi, G. Modeling and Experimental Activities on a Small-scale Sliding Vane Pump for ORC-based Waste Heat Recovery Applications. *Energy Procedia* **2016**, *101*, 1240–1247. [CrossRef]
31. Bianchi, G.; Fatigati, F.; Murgia, S.; Cipollone, R. Design and analysis of a sliding vane pump for waste heat to power conversion systems using organic fluids. *Appl. Therm. Eng.* **2017**, *124*, 1038–1048. [CrossRef]
32. Yang, Y.; Zhang, H.; Tian, G.; Xu, Y.; Wang, C.; Gao, J. Performance Analysis of a Multistage Centrifugal Pump Used in an Organic Rankine Cycle (ORC) System under Various Condensation Conditions. *J. Therm. Sci.* **2019**, *28*. [CrossRef]
33. Liu, L.; Zhu, T.; Wang, T.; Gao, N. Experimental investigation on the effect of working fluid charge in a small-scale Organic Rankine Cycle under off-design conditions. *Energy* **2019**, *174*, 664–677. [CrossRef]
34. Fornarelli, F.; Lippolis, A.; Oresta, P.; Posa, A. Investigation of a pressure compensated vane pump. *Energy Procedia* **2018**, *148*, 194–201. [CrossRef]
35. Cipollone, R.; Bianchi, G.; Di Battista, D.; Fatigati, F. Fuel economy benefits of a new engine cooling pump based on sliding vane technology with variable eccentricity. *Energy Procedia* **2015**, *82*, 265–272. [CrossRef]
36. Villani, M.; Tribioli, L. Comparison of different layouts for the integration of an organic Rankine cycle unit in electrified powertrains of heavy duty Diesel trucks. *Energy Convers. Manag.* **2019**, *187*, 248–261. [CrossRef]
37. Liu, C.; Gao, T. Off-design performance analysis of basic ORC, ORC using zeotropic mixtures and composition-adjustable ORC under optimal control strategy. *Energy* **2019**, *171*, 95–108. [CrossRef]
38. Peralez, J.; Nadri, M.; Dufour, P.; Tona, P.; Sciarretta, A. Organic Rankine Cycle for Vehicles: Control Design and Experimental Results. IEEE Transactions on Control Systems Technology. *Inst. Electr. Electron. Eng.* **2017**, *25*, 952–965.
39. Guillaume, L. On the Design of Waste Heat Recovery Organic Rankine Cycle Systems for Engines of Long-Haul Trucks. Ph.D. Thesis, Université de Liège, Liège, Belgique, 2017.
40. Zhang, J.; Zhang, W.; Hou, G.; Fang, F. Dynamic modeling and multivariable control of organic Rankine cycles in waste heat utilizing processes. *Comput. Math. Appl.* **2012**, *64*, 908–921. [CrossRef]
41. Manente, G.; Toffolo, A.; Lazzaretto, A.; Paci, M. An organic rankine cycle off-design model for the search of the optimal control strategy. *Energy* **2013**, *58*, 97–106. [CrossRef]
42. Imran, M.; Haglind, F.; Lemort, V.; Meroni, A. Multi-objective optimization of organic Rankine cycle power systems for waste heat recovery on heavy-duty vehicles. In Proceedings of the 31st International Conference on Efficiency, Cost, Optimization, Simulation and Environmental Impact of Energy Systems (ECOS 2018), Guimaraes, Portugal, 17–22 June 2018.
43. Wei, D.; Lu, X.; Lu, Z.; Gu, J. Dynamic modeling and simulation of an Organic Rankine Cycle (ORC) system for waste heat recovery. *Appl. Therm. Eng.* **2008**, *28*, 1216–1224. [CrossRef]
44. Marchionni, M.; Bianchi, G.; Karvountzis-Kontakiotis, A.; Pesyridis, A.; Tassou, S.A. An appraisal of proportional integral control strategies for small scale waste heat to power conversion units based on Organic Rankine Cycles. *Energy* **2018**, *163*, 1062–1076. [CrossRef]
45. Peralez, J. Rankine Cycle for Waste Heat Recovery on Board Vehicles: Control and Energy Management. Ph.D. Thesis, Université Claude Bernard Lyon 1, Villeurbanne, France, 2015.
46. Jensen, J.M.; Tummescheit, H. Moving boundary models for dynamic simulations of two-phase flows. In Proceedings of the 2nd International Modelica Conference, Oberpfaffenhofen, Germany, 18–19 March 2002; pp. 235–244.
47. Grelet, V. Rankine Cycle-Based Waste Heat Recovery System Applied to Heavy Duty Vehicles: Topological Optimization and Model-Based Control. Ph.D. Thesis, Université de Liège, Liège, Belgique, 2016.
48. Fatigati, F.; Bianchi, G.; Cipollone, R. Development and numerical modelling of a supercharging technique for positive displacement expanders. *Appl. Therm. Eng.* **2018**, *140*, 208–216. [CrossRef]
49. Fatigati, F.; di Bartolomeo, M.; Cipollone, R. Experimental and numerical characterization of a positive displacement vane expander with an auxiliary injection port for an ORC-based power unit. *Energy Procedia* **2018**, *148*, 830–837. [CrossRef]
50. Cipollone, R.; Bianchi, G.; Gualtieri, A.; di Battista, D.; Mauriello, M.; Fatigati, F. Development of an Organic Rankine Cycle system for exhaust energy recovery in internal combustion engines. *J. Phys. Conf. Ser.* **2015**, *655*, 012015. [CrossRef]
51. Fatigati, F.; di Bartolomeo, M.; Cipollone, R. Dual intake rotary vane expander technology: Experimental and theoretical assessment. *Energy Convers. Manag.* **2019**, *186*, 156–167. [CrossRef]

52. GT-Suite Flow Theory Manual. Version 2019. Gamma Technologies LLC. Available online: https://www.gtisoft.com (accessed on 1 May 2019).
53. Quoilin, S.; Lemort, V.; Lebrun, J. Experimental study and modeling of an Organic Rankine Cycle using scroll expander. *Appl. Energy* **2010**, *87*, 1260–1268. [CrossRef]